# Stretchable, skin-conformal microscale surface-emitting lasers with dynamically tunable spectral and directional selectivity •

Cite as: Appl. Phys. Lett. 114, 041103 (2019); https://doi.org/10.1063/1.5080947 Submitted: 12 November 2018 . Accepted: 14 December 2018 . Published Online: 29 January 2019

Dongseok Kang, Huandong Chen, and Jongseung Yoon 🗓

### **COLLECTIONS**

- This paper was selected as Featured
- This paper was selected as Scilight







### ARTICLES YOU MAY BE INTERESTED IN

Researchers create stretchable, skin-conformable microscale surface-emitting laser Scilight 2019, 050003 (2019); https://doi.org/10.1063/1.5090278

Tunable polarization singularity array enabled using superposition of vector curvilinear beams Applied Physics Letters 114, 041101 (2019); https://doi.org/10.1063/1.5082842

Controllable excitation of quasi-linear and bullet modes in a spin-Hall nano-oscillator Applied Physics Letters 114, 042403 (2019); https://doi.org/10.1063/1.5064841

# Lock-in Amplifiers up to 600 MHz







## Stretchable, skin-conformal microscale surfaceemitting lasers with dynamically tunable spectral and directional selectivity © •

Cite as: Appl. Phys. Lett. **114**, 041103 (2019); doi: 10.1063/1.5080947 Submitted: 12 November 2018 · Accepted: 14 December 2018 · Published Online: 29 January 2019







Dongseok Kang, Huandong Chen, and Jongseung Yoon 1.2,a) [D

### **AFFILIATIONS**

- Department of Chemical Engineering and Materials Science, University of Southern California, Los Angeles, California 90089, USA
- Department of Electrical Engineering, University of Southern California, Los Angeles, California 90089, USA
- a) Author to whom correspondence should be addressed: js.yoon@usc.edu

### **ABSTRACT**

Coherent, monochromatic light sources that can intimately integrate with human body and yet offer state-of-the-art optoelectronic performance will create new opportunities in wearable and implantable electronics for a wide range of applications from personalized health monitoring, light therapy, to three-dimensional sensing and security. Here, we report stretchable, electrically driven surface-emitting microlasers capable of being conformally integrated on soft, curvilinear surfaces of biological tissues and providing wafer-level performance under mechanical and thermal environments relevant to skin physiology. GaAs-based microscale 850-nm vertical-cavity surface-emitting lasers derived from epitaxially grown source materials are integrated on a thin, elastomeric membrane in stretchable and thermally robust configurations enabled by printing-based heterogeneous material assemblies. The resulting stretchable, electrically pumped microlasers offer a stable continuous-wave operation under both uniaxial and biaxial tensile strains up to ~120% in air as well as on the human skin, where the synergistic choices of mechanical strain and underlying heat-transfer medium provide versatile routes to dynamically control the spectral and directional characteristics of lasing.

Published under license by AIP Publishing. https://doi.org/10.1063/1.5080947

Vertical-cavity surface-emitting lasers (VCSELs) have been in the core of numerous important technologies including fiberoptic data communication, infrared illumination, chip-scale atomic clocks, three-dimensional (3D) sensing, and others. 1-1 More recently, VCSELs have also broadened their utilities in biomedical imaging and sensing, where they served as deep-red or near-infrared coherent light sources for optical processes involving fluorescence, absorption, and/or scattering.<sup>6–10</sup> One of the compelling advances includes VCSEL-based implantable fluorescence sensors using monolithically integrated 675 nm VCSELs and GaAs PIN photodiodes for in vivo detection of tumor-targeted molecular probes in animal models.<sup>8–10</sup> Although well-suited for many applications, such chip-based optoelectronic sensors, however, are built on a rigid and planar semiconductor wafer and thus inherently limited for intimate and conformal integration onto soft, curvilinear surfaces of biological tissues. In addition, the areal coverage of constituting device components is often restricted, making it difficult to realize large-scale arrays desired for spatio-temporal mapping of

sensing signals. To address these difficulties, Kang et al. reported materials and fabrication strategies for the defect-free release of microscale vertical cavity surface emitting lasers (micro-VCSELs) from a GaAs growth wafer and their device- and circuit-level implementation on various unconventional substrates. 11-13 Key aspects in this approach include an epitaxial design that incorporates "sacrificial" (Al<sub>0.95</sub>Ga<sub>0.05</sub>As) and "etchstop" (Al<sub>0.40</sub>Ga<sub>0.60</sub>As) layers, specialized etching processes for preventing unwanted damages to distributed Bragg reflectors (DBRs) and active region, and printing-based high-throughput material integration on unlimited choices of a target substrate with a precisely controlled spatial layout. 14-16 More recently, Kang et al. reported fabrication schemes that can circumvent challenges in thermal management of micro-VCSELs operating on substrates with intrinsically low thermal conductivity such as plastics or glass, where a composite structure to accelerate the heat removal from the laser cavity was incorporated to preserve the wafer-level performance of printed micro-VCSELs.<sup>12</sup> Building on these complementary advances, herein we report

stretchable platforms of surface-emitting microlasers implemented on an ultra-compliant, bio-compatible membrane, capable of offering stable continuous-wave (CW) performance under mechanical and thermal environments relevant to their operation on the human skin as well as in air (i.e., free-standing), while allowing the dynamic control of spectral and directional characteristics of lasing by synergistic choices of mechanical strain and underlying heat-transfer medium. In the following, we present systematic studies on electrical, optical, mechanical, and thermal properties of stretchable surface-emitting microlasers, together with numerical thermal modeling, highlighting essential aspects of underlying materials science as well as thermal and strain engineering exploited to enable unique capabilities of the reported system.

Figure 1 schematically illustrates fabrication procedures to construct mechanically and thermally optimized assemblies of stretchable surface-emitting microlasers. The fabrication begins with the spin-coating and thermal curing of polyimide (PI:  $\sim$ 4.5  $\mu$ m) on a double-layer sheet (35  $\mu$ m/5  $\mu$ m) of copper. The PI-covered surface of the copper sheet was laminated on a slide glass coated with cured polydimethylsiloxane (PDMS). The thicker copper layer was then peeled off to yield a thin ( $\sim$ 5  $\mu$ m) copper film on a temporary carrier substrate (PI/PDMS/glass). Subsequently, the copper film was patterned by photolithography and wet chemical etching to yield square-shaped islands  $(\sim 1 \times 1 \times 0.005 \,\mathrm{mm}^3)$  that can serve as a heat spreading medium for printed microlasers. 12 Microscale ( $\sim 250 \times 250 \ \mu \text{m}^2$ ) VCSELs with an aperture size of  $\sim$ 22 × 22  $\mu$ m<sup>2</sup> fabricated by previously reported procedures<sup>11,12</sup> were released from the GaAs growth wafer and transferred individually onto the pre-patterned copper islands using a PDMS stamp with relief features and a thin ( $\sim$ 1  $\mu$ m) photocurable polymer as an adhesive.<sup>17</sup> After the printing, photolithography and electron-beam evaporation of metals (Cr/Cu/Au = 15 nm/2000 nm/100 nm) defined polymeric "via" and serpentine-shaped metal interconnects (Fig. S1), followed by the spin-coating of PI ( $\sim$ 4.5  $\mu$ m), photolithography, and oxygen reactive ion etching (O2 RIE) to implement the neutral mechanical plane layout for strain isolation. 18,19 The mesh-like interconnected arrays of micro-VCSELs were then released from the carrier substrate and transferred onto a thin

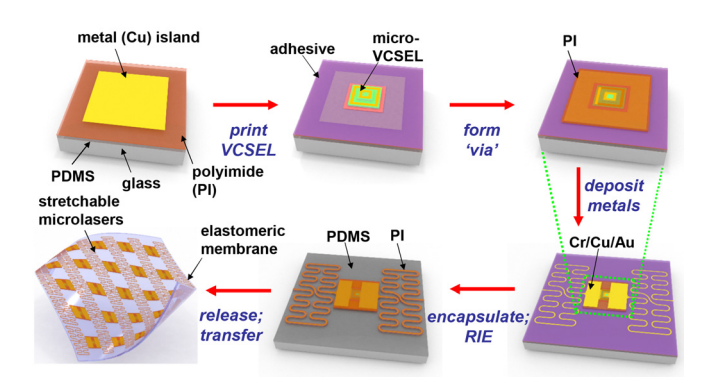


**FIG. 1.** Schematic illustration of fabrication processes for stretchable assemblies of microscale vertical cavity surface emitting lasers (micro-VCSELs).

(~0.8–1.0 mm), unstrained elastomeric membrane (Ecoflex<sup>TM</sup>) to produce a stretchable embodiment of surface-emitting microlasers in a thermally and mechanically optimized configuration (Fig. S2). In the present work, we adopted a coplanar "island-bridge" layout, <sup>16,20</sup> where the entire bottom surface of the PI-encapsulated mesh was laminated and bonded to the elastomeric substrate.

Given that the rubber substrate employed in this study has over two orders of magnitude lower thermal conductivity than the growth wafer, 11,12 appropriate thermal management is crucial to ensure the undiminished performance and reliability of stretchable microlasers. In this regard, we adopted a previously reported "thermally engineered composite substrate" for flexible micro-VCSELs, <sup>12</sup> where thin (approximately a few microns) metals were incorporated as a heat spreading medium between the released micro-VCSEL and the polymeric substrate to promote the cooling of the laser cavity and avoid thermally induced spectral mismatch and degradation of output characteristics. To examine the effectiveness of thermal management, electrical and optical properties of printed micro-VCSELs were characterized at respective fabrication steps, where the maximum output power of lasing was measured to compare the efficacy of heat dissipation from the laser cavity. Figure 2(a) shows the output optical power (L) of an individual micro-VCSEL as a function of driving current (I) at various stages of device fabrication, including after (i) the printing on a temporary carrier substrate (i.e., Cu/PI/PDMS/glass), (ii) the formation of polymeric via, (iii) the deposition of metal interconnects, (iv) the encapsulation, and (v) the transfer onto an elastomeric substrate (i.e., Ecoflex) (Fig. S3). In all these measurements, samples were placed on a metallic stage that can serve as a passive heat sink. The output optical power of printed micro-VCSELs increased after the deposition of PI [step (ii)] and interconnect metals [step (iii)], as the additionally deposited materials served as heat-transfer media to help extract the heat from the laser cavity more effectively. The increased output power with the coating of a polymeric encapsulation layer [step (iv)] is primarily due to the reduced refractive index mismatch between the semiconductor and air at the aperture of micro-VCSEL to yield the enhanced out-coupling of lasing emission. On the other hand, the maximum output power moderately decreased by ~21% after the transfer to the stretchable substrate (i.e., Ecoflex) because of the comparatively less efficient heat removal associated with a low thermal conductivity and a high thermal resistance ( $R_{th} \sim t/k$ , t: thickness, k: thermal conductivity) of the polymeric membrane. The corresponding current (I)-voltage (V) characteristics [Fig. 2(b)] are consistent with these observations, where the voltage at a fixed current substantially increased after the step (iii) owing to the increased series resistance associated with metal interconnects. The decreased voltage at a constant current after the transfer to the elastomeric substrate [i.e., step (v)] suggests thermally induced reduction of series resistance in the DBR.<sup>21,22</sup> numerical modeling of heat transfer also supports these analyses. The steady-state temperature distribution of printed micro-VCSELs was calculated by COMSOL Multiphysics® software using a single volumetric heat source within the active region (33  $\times$  33  $\times$  0.25  $\mu$ m<sup>3</sup>) of a micro-VCSEL, <sup>12</sup> where a natural

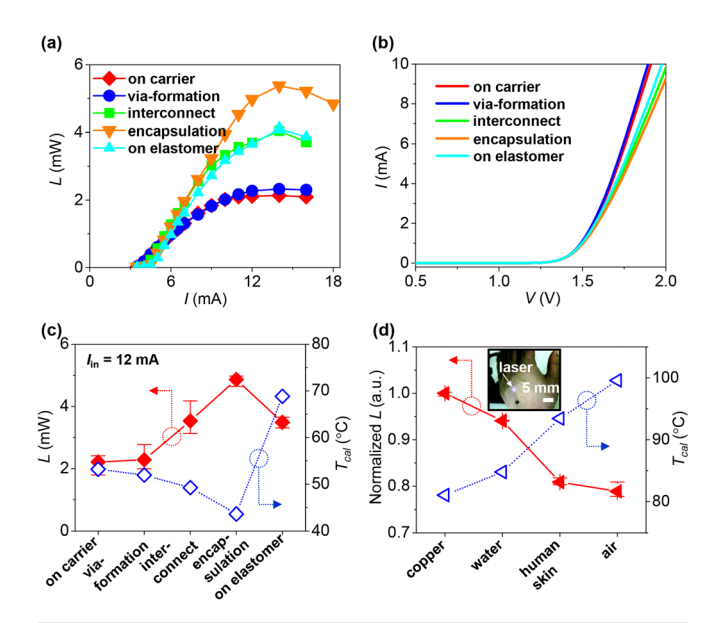


FIG. 2. (a) Representative output optical power (L) of an individual micro-VCSEL as a function of driving current (/) at various steps of device fabrication for stretchable microlasers, including after (i) the printing on a temporary carrier substrate (i.e., Cu/PI/PDMS/glass), (ii) the formation of polymeric "via," (iii) the deposition of metal interconnects, (iv) the encapsulation, and (v) the transfer onto an elastomeric substrate (i.e., Ecoflex). (b) Corresponding current (I)-voltage (V) curves of an individual micro-VCSEL at respective fabrication steps. (c) Calculated steady-state temperature (open diamond) of the active region of an individual micro-VCSEL at various fabrication steps at the input current of 12 mA, obtained from 3D numerical thermal modeling by COMSOL Multiphysics® software using a single volumetric heat source within the active region of the micro-VCSEL. Corresponding values of measured output optical power (filled diamond) of micro-VCSELs are also shown. (d) Normalized output power (filled triangle) of a stretchable micro-VCSEL at various choices of underlying media directly underneath the bottom surface of the elastomeric support, including copper, water, human skin (dorsal surface of hand), and air, measured at the input current of 12 mA. Calculated values (open triangle) of steady-state temperature of the active region of a micro-VCSEL from 3D numerical thermal modeling also appear for comparison. The inset shows a photographic image of a stretchable micro-VCSEL on the dorsal surface of human hand.

convection boundary condition in air  $[h=25 \text{ W/(m}^2 \text{ K}), T_{\text{ext}} = 20 \,^{\circ}\text{C}]$  was employed at all solid/air interfaces except the bottom of the elastomeric membrane that assumed either a constant temperature boundary condition for solid or a natural convection boundary condition for fluidic (i.e., liquid and vapor) medium. To accurately capture the phenomena, the input power of the heat source in the simulation was independently determined for each fabrication step from the experimentally estimated dissipated power ( $P_{diss} = I \times V - L$ ) measured at the input current of 12 mA. As summarized in Figs. 2(c), S4 and Table S1, the calculated steady-state temperature (open diamond) of micro-VCSELs was in semi-quantitative agreement with the measured variation of output power (filled diamond) of micro-VCSELs at respective fabrication steps.

Given that the thermal resistance of an elastomeric substrate is high, the medium underneath the stretchable assembly also plays a critical role in the heat management of printed micro-VCSELs. Of particular interest is the thermal environment

relevant to applications on the human skin, where microlasers are employed as coherent light sources for noninvasive optical sensing. We examined this aspect by considering various types of underlying media below the bottom surface of the elastomer in experiments as well as numerical modeling, including copper, water, human skin (i.e., dorsal surface of hand), as well as air, where the temperature of all media except the human skin  $(T = 34 \,^{\circ}C)^{23}$  was assumed to be at ambient temperature (~20 °C) [Figs. 2(d), S5, and Table S2]. As expected, the highest output power (~3.3 mW) was obtained when copper was used as a substrate medium because of its high thermal conductivity and correspondingly rapid heat extraction. Compared to this reference case, the output power decreased by  $\sim$ 4,  $\sim$ 19, and ~24% when employing water, human skin, and air as a substrate medium, respectively, on the order of decreasing the effectiveness of heat extraction. Notably, although the human skin and air are not as effective heat sink as copper, the output power of micro-VCSEL in the stretchable assembly was maintained at the level of  $\sim$ 81% (i.e.,  $\sim$ 2.7 mW) and  $\sim$ 76% (i.e.,  $\sim$ 2.5 mW) of the reference, respectively, which are sufficiently high for many non-invasive physiological sensors on the human skin including laser Doppler flowmetry and pulse oximetry. 24,25 These experimental results (filled triangle) are also consistent with the trend of calculated steady-state temperature [open triangle in Figs. 2(d) and S6].

Lasing characteristics of stretchable assembly of microlasers were examined under uniaxial and biaxial tensile strains using a home-made stretching set-up (Fig. S7), where both air and water were employed as a medium underneath the elastomeric substrate. In the present study, the performance of a micro-VCSEL at the central (i.e., 3rd) position of a 1 × 5 interconnected array was examined, while metal islands at the 1st, 2nd, 4th, and 5th positions were electrically connected in series without printed devices to simplify the analysis. Figures 3(a)-3(c) show optical micrographs of the above-described stretchable VCSEL assembly under uniaxial tensile deformation  $[\varepsilon_x = (l_x)]$  $-l_{x0}$ )/ $l_{x0} \times 100$ ;  $\varepsilon_v = (l_v - l_{v0})/l_{v0} \times 100$ ;  $\varepsilon_x$  ( $\varepsilon_v$ ): tensile strain,  $l_{x0}$  $(l_{v0})$ : initial length,  $l_x$   $(l_v)$ : length after the deformation] along [x-direction, Fig. 3(a)] and perpendicular to [y-direction, Fig. 3(b)] the longitudinal direction of a row, as well as biaxial tensile deformation [ $\varepsilon_x = \varepsilon_y$ , Fig. 3(c)] at various levels of strain, all conducted in air. With the coplanar "island-bridge" design and mechanical properties of elastomeric membrane employed in this study, the serpentine-shaped metal interconnects allowed the system to accommodate uniaxial and biaxial tensile strains up to ~120% and ~60%, respectively, without causing permanent deterioration of lasing functionality, supporting their mechanical durability in skin-laminated applications that demand elastic behaviors for strains of tens of percent.<sup>26</sup> Notably, as the strain level increased, the output power of micro-VCSEL gradually decreased in all deformation modes examined in this study (e.g., by ~21% at the uniaxial strain of 120%), while the rate of decrease was substantially higher under biaxial stretching [Fig. 3(d)]. We attribute this attenuation of output power of lasing to the reduced thickness of the elastomeric membrane upon stretching and resultant elevation of temperature in the laser cavity. Because of the comparatively low heat

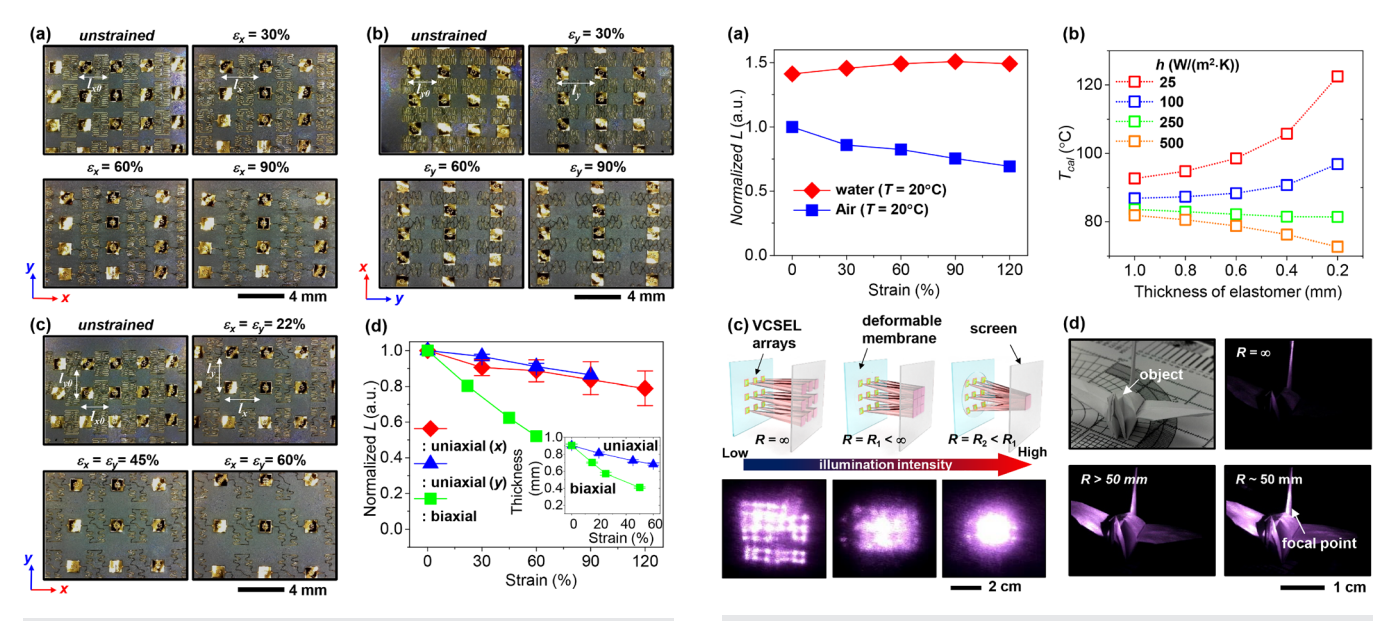


**FIG. 3.** Optical micrographs of stretchable VCSEL assembly under uniaxial tensile  $(\varepsilon_x = (l_x - l_{x0})/l_{x0} \times 100; \ \varepsilon_y = (l_y - l_{y0})/l_{y0} \times 100; \ l_{x0} \ (l_{y0}):$  initial length,  $l_x \ (l_y):$  length after the deformation) (a) along (x-direction) and (b) perpendicular to (y-direction) the longitudinal direction of a row, as well as (c) biaxial tensile deformation  $(\varepsilon_x = \varepsilon_y)$  at various strain levels, all measured in air. (d) Corresponding normalized output optical power of an individual micro-VCSEL at the input current of 12 mA as a function of applied strain. The inset shows the measured thickness of an elastomeric membrane under uniaxial and biaxial stretching at various levels of tensile strain. The initial thickness of the membrane was  $\sim$ 0.9 mm.

transfer coefficient of air, most of heat spreading from a local heat source (i.e., VCSEL) predominantly occurs by the mechanism of thermal conduction through a solid-state medium (i.e., elastomer). As the thickness of elastomer decreases upon stretching [the inset of Fig. 3(d)], the thermal resistance in "inplane" directions increases, thereby leading to the elevation of cavity temperature and the corresponding decrease in lasing output power. The rate of change in the cavity temperature and output power is higher under the biaxial stretching owing to the faster decrease in elastomer thickness [the inset of Fig. 3(d)]. Nonetheless, the current-voltage characteristics of a stretchable VCSEL remained nearly unchanged under the tensile test (Fig. S8), confirming the robustness of strain-isolation with the serpentine-shaped metal interconnects.

Such stretchable, surface-emitting microlasers implemented on a thin, elastomeric membrane can provide versatile routes to dynamically tune the spectral and directional characteristics of lasing. As previously noted, the strain-induced thickness variation of elastomeric support can be employed to reversibly tune the temperature of the laser cavity and thus emission characteristics of lasing. Additionally, the choice of underlying heat transfer medium plays an important role in determining the spectral response of microlasers under strained conditions. As depicted in Fig. 4(a), when water ( $T=20\,^{\circ}\text{C}$ ) was employed as a medium directly underneath the stretchable substrate during the tensile test, VCSEL's output power was higher than in air by  $\sim$ 41% at the unstrained condition ( $\epsilon=0$ ) and was

FIG. 4. (a) Normalized optical output power of a stretchable micro-VCSEL measured under various levels of uniaxial tensile strains at an input current of 12 mA, with water (red data) or air (blue data) as underlying heat transfer media, respectively. (b) Calculated steady-state temperature of a micro-VCSEL as a function of thickness of an elastomeric substrate at various values of heat transfer coefficient of the underlying medium, obtained from 3D numerical thermal modeling. (c) Schematic illustration of a collection of lasing beams emitted from a  $3\times 3$  array of microlasers implemented on an elastomeric support. By changing the radius of curvature (R) of the membrane from flat  $(R = \infty)$  to concave states  $(R = R_2 < R_1 < \infty)$ , the direction and intensity of laser illumination can be dynamically changed. The inset shows the corresponding photographic images of lasing beams at flat (left) and concave states (center and right), measured at the input current of 12 mA. (d) Photographic images of a paper bird (upper-left) as a target object illuminated by 5 × 3 array of stretchable micro-VCSELs at three different R of the elastomeric support, where the VCSEL array with the applied current of 12 mA was placed at a distance of  $\sim$ 50 mm from the object and at an angle of  $\sim$ 60° from the surface normal (Fig. S12). At  $R=\infty$  (i.e., flat state, *upper-right*), the illumination intensity to the object was not sufficiently high for imaging. As the radius of curvature decreased (lower-left) and reached ~50 mm (lower-right), the lasing beams were focused at the paper bird to produce higher illumination intensity for imaging.

increased with applied mechanical strains (i.e.,  $\varepsilon > 0$ ), indicating that the cavity temperature of VCSEL was lowered by thinning the elastomeric membrane. This opposite trend can be explained by a larger value of the heat transfer coefficient of water than air, which increased the contribution of convective heat transfer to the heat extraction from the laser cavity. Accordingly, the decrease in the elastomer thickness upon stretching lowers the thermal resistance along the thickness direction and facilitates the heat extraction via convective heat transfer at the bottom surface of the membrane, thereby resulting in the increased output power of lasing. This analysis is also consistent with the trends obtained from numerical thermal modeling. As summarized in Fig. 4(b), the temperature of the laser cavity can be increased, decreased, or unchanged upon decreasing the thickness of elastomeric support depending on the choice of heat transfer coefficient of underlying medium. Such strain-induced control of cavity temperature also translates directly to the shift of the spectral position of lasing output (Fig. S9), where the type of underlying heat transfer medium

determines the direction and magnitude of spectral shift. The peak wavelength of lasing moves to a longer (shorter) wavelength range upon stretching when the heat transfer coefficient of the underlying medium is relatively small (large) and the conduction (convection) is thus a dominant mechanism of heat extraction. With an appropriate choice of underlying medium, the spectral shift of stretchable microlasers under strained conditions can be also eliminated. Another potential advantage of the reported stretchable microlasers is to dynamically tune the direction of laser emission by the controlled deformation of elastomeric support. To demonstrate this capability, the stretchable assembly of interconnected microlasers was mounted on a custom-built fluidic chamber with a circular hole (Figs. S10 and S11), where the curvature of the elastomeric membrane can be made progressively concave (or convex) by applying a negative (or positive) pressure to the chamber. Accordingly, the direction of laser illumination converges (diverge) to increase (decrease) the illumination intensity at a local point in space [Fig. 4(c)]. Figure 4(d) shows photographic images of a paper bird as a target object for detection illuminated by 850 nm laser, where a  $5 \times 3$ array of stretchable micro-VCSELs was placed at a distance of  $\sim$ 50 mm from the object at an angle of  $\sim$ 60° from the surface normal (Fig. S12). While the illumination intensity to the object is weak at a flat state of the elastomeric support, lasing beams are focused at the paper bird to produce a brighter illumination for imaging as the radius of curvature decreased to  $\sim$ 50 mm.

In summary, stretchable, surface-emitting microlasers capable of conformally adherent on soft, curvilinear surfaces and yet providing wafer-level performance under mechanical and thermal environments relevant to skin physiology have been demonstrated. Such stretchable, electrically driven platforms of coherent light sources have great potential to create a wide range of new capabilities in wearable electronics, <sup>27–29</sup> noninvasive health monitoring, <sup>30</sup> therapeutics, <sup>31</sup> and advanced 3D sensing for security and surveillance, <sup>32</sup> where we expect the work presented here will serve as a foundation for future research and development.

See supplementary material for additional details of fabrication procedures, electrical and optical characterization, numerical thermal modeling, mechanical test, and pneumatically controlled lasing characteristics.

We gratefully acknowledge support from the DARPA YFA Program (N66001-12-1-4244) and National Science Foundation (CBET-1707169).

### **REFERENCES**

- <sup>1</sup>K. Iga, Proc. IEEE **101**, 2229 (2013).
- <sup>2</sup>J. S. Harris, T. O'Sullivan, T. Sarmiento, M. M. Lee, and S. Vo, Semicond. Sci. Technol. 26, 014010 (2011).
- <sup>3</sup>E. Karl Joachim, M. Rainer, and M. Holger, Jpn. J. Appl. Phys. Part 1 57, 08PA02 (2018).
- <sup>4</sup>K. D. Choquette and H. Q. Hou, Proc. IEEE **85**, 1730 (1997).
- <sup>5</sup>A. Larsson, IEEE J. Select. Top. Quantum Electron. 17, 1552 (2011).
- <sup>6</sup>C. Liu, H. Cao, and M. A. Choma, Opt. Lett. **41**, 4775 (2016).
- <sup>7</sup>A. Mowla, T. Taimre, K. Bertling, S. Wilson, and A. D. Rakić, in Electronics Letters (Institution of Engineering and Technology, 2018), Vol. 54, p. 196.

- <sup>8</sup>T. O'Sullivan, E. A. Munro, N. Parashurama, C. Conca, S. S. Gambhir, J. S. Harris, and O. Levi, Opt. Express 18, 12513 (2010).
- <sup>9</sup>N. Parashurama, T. D. O'Sullivan, A. De La Zerda, P. El Kalassi, S. Cho, H. G. Liu, R. Teed, H. Levy, J. Rosenberg, Z. Cheng, O. Levi, J. S. Harris, and S. S. Gambhir, J. Biomed. Opt. 17, 117004 (2012).
- <sup>10</sup>T. D. O'Sullivan, R. T. Heitz, N. Parashurama, D. B. Barkin, B. A. Wooley, S. S. Gambhir, J. S. Harris, and O. Levi, Biomed. Opt. Express 4, 1332 (2013).
- <sup>11</sup>D. Kang, S. M. Lee, Z. W. Li, A. Seyedi, J. O'Brien, J. L. Xiao, and J. Yoon, Adv. Opt. Mater. 2, 373 (2014).
- <sup>12</sup>D. Kang, S. M. Lee, A. Kwong, and J. Yoon, Adv. Opt. Mater. 3, 1072 (2015).
- <sup>13</sup>D. Kang, B. Gai, B. Thompson, S.-M. Lee, N. Malmstadt, and J. Yoon, ACS Photonics 3, 912 (2016).
- <sup>14</sup>A. Carlson, A. M. Bowen, Y. Huang, R. G. Nuzzo, and J. A. Rogers, Adv. Mater. 24, 5284 (2012).
- 15B. Corbett, R. Loi, W. Zhou, D. Liu, and Z. Ma, Prog. Quantum Electron. 52,
- <sup>16</sup>J. Yoon, S.-M. Lee, D. Kang, M. A. Meitl, C. A. Bower, and J. A. Rogers, Adv. Opt. Mater. **3**, 1313 (2015).
- <sup>17</sup>B. Gai, Y. Sun, H. Lim, H. Chen, J. Faucher, M. L. Lee, and J. Yoon, ACS Nano 11, 992 (2017).
- <sup>18</sup>S.-M. Lee, A. Kwong, D. Jung, J. Faucher, R. Biswas, L. Shen, D. Kang, M. L. Lee, and J. Yoon, ACS Nano 9, 10356 (2015).
- <sup>19</sup>D. Kang, J. L. Young, H. Lim, W. E. Klein, H. Chen, Y. Xi, B. Gai, T. G. Deutsch, and J. Yoon, Nat. Energy 2, 17043 (2017).
- <sup>20</sup>S. Xu, Y. Zhang, J. Cho, J. Lee, X. Huang, L. Jia, J. A. Fan, Y. Su, J. Su, H. Zhang, H. Cheng, B. Lu, C. Yu, C. Chuang, T.-I. Kim, T. Song, K. Shigeta, S. Kang, C. Dagdeviren, I. Petrov, P. V. Braun, Y. Huang, U. Paik, and J. A. Rogers, Nat. Commun. 4, 1543 (2013).
- <sup>21</sup>K. Tai, L. Yang, Y. H. Wang, J. D. Wynn, and A. Y. Cho, Appl. Phys. Lett. 56, 2496 (1990).
- <sup>22</sup>K. Kurihara, T. Numai, I. Ogura, A. Yasuda, M. Sugimoto, and K. Kasahara, J. Appl. Phys. **73**, 21 (1993).
- <sup>23</sup>F. Suarez, A. Nozariasbmarz, D. Vashaee, and M. C. Öztürk, Energy Environ. Sci. 9, 2099 (2016).
- <sup>24</sup>D. Kollmann, W. K. Hogan, C. Steidl, M. K. Hibbs-Brenner, D. S. Hedin, and P. A. Lichter, in VCSEL Based, Wearable, Continuously Monitoring Pulse Oximeter (IEEE, 2013), p. 4156.
- <sup>25</sup>A. N. Serov, J. Nieland, S. Oosterbaan, F. F. M. D. Mul, H. V. Kranenburg, H. H. P. T. Bekman, and W. Steenbergen, IEEE Trans. Biomed. Eng. **53**, 2067 (2006).
- <sup>26</sup>D.-H. Kim, N. Lu, R. Ma, Y.-S. Kim, R.-H. Kim, S. Wang, J. Wu, S. M. Won, H. Tao, A. Islam, K. J. Yu, T.-I. Kim, R. Chowdhury, M. Ying, L. Xu, M. Li, H.-J. Chung, H. Keum, M. McCormick, P. Liu, Y.-W. Zhang, F. G. Omenetto, Y. Huang, T. Coleman, and J. A. Rogers, Science 333, 838 (2011).
- <sup>27</sup>M. Kaltenbrunner, T. Sekitani, J. Reeder, T. Yokota, K. Kuribara, T. Tokuhara, M. Drack, R. Schwodiauer, I. Graz, S. Bauer-Gogonea, S. Bauer, and T. Someya, Nature 499, 458 (2013).
- <sup>28</sup>J. H. Choi, E. H. Cho, Y. S. Lee, M.-B. Shim, H. Y. Ahn, C.-W. Baik, E. H. Lee, K. Kim, T.-H. Kim, S. Kim, K.-S. Cho, J. Yoon, M. Kim, and S. Hwang, Adv. Opt. Mater. 2, 267 (2014).
- <sup>29</sup> R.-H. Kim, D.-H. Kim, J. Xiao, B. H. Kim, S.-I. Park, B. Panilaitis, R. Ghaffari, J. Yao, M. Li, Z. Liu, V. Malyarchuk, D. G. Kim, A.-P. Le, R. G. Nuzzo, D. L. Kaplan, F. G. Omenetto, Y. Huang, Z. Kang, and J. A. Rogers, Nat. Mater. 9, 929 (2010).
- <sup>30</sup>K.-I. Jang, S. Y. Han, S. Xu, K. E. Mathewson, Y. Zhang, J.-W. Jeong, G.-T. Kim, R. C. Webb, J. W. Lee, T. J. Dawidczyk, R. H. Kim, Y. M. Song, W.-H. Yeo, S. Kim, H. Cheng, S. I. Rhee, J. Chung, B. Kim, H. U. Chung, D. Lee, Y. Yang, M. Cho, J. G. Gaspar, R. Carbonari, M. Fabiani, G. Gratton, Y. Huang, and J. A. Rogers, Nat. Commun. 5, 4779 (2014).
- <sup>31</sup>D. Son, J. Lee, S. Qiao, R. Ghaffari, J. Kim, J. E. Lee, C. Song, S. J. Kim, D. J. Lee, S. W. Jun, S. Yang, M. Park, J. Shin, K. Do, M. Lee, K. Kang, C. S. Hwang, N. S. Lu, T. Hyeon, and D. H. Kim, Nat. Nanotechnol. 9, 397 (2014).
- <sup>32</sup>W. Osten and W. P. O. Jueptner, in New Light Sources and Sensors for Active Optical 3D Inspection (SPIE, 1999), p. 14.